Korean Journal of Remote Sensing, Vol.27, No.3, 2011, pp.277~288

Development of Snowfall Retrieval Algorithm by Combining Measurements from CloudSat, AQUA and NOAA Satellites for the Korean Peninsula

Young-Seup Kim †, Na-Ri Kim, Kyung-Won Park

Department of Spatial Information Engineering, Pukyong National University,
Daeyeon 3-dong Nam-gu, Busan 608-737, Korea

Abstract : Cloudsat satellite data is sensitive to snowfall and collected during each month beginning with Dec 2007 and ending Feb 2008. In this study, we attempt to develop a snowfall retrieval algorithm using a combination of radiometer and cloud radar data. We trained data from the relation between brightness temperature measurements from NOAA's Advanced Microwave Sounder Unit-B(AMSU-B) and the radar reflectivity of the 2B-GEOPROF product from W-band(94 GHz) cloud radar onboard Cloudsat and applied it to the Korea peninsula. We use a principal components analysis to quantify the variations that are the result of the radiometric signatures of snowfall from those of the surface. Finally, we quantify the correlation between the higher principal component (orthogonal to surface variability) of the microwave radiances and the precipitation-sensitive CloudSat radar reflectivities. This work summarizes the results of applying this approach to observations over the East Sea during Feb. 2008. The retrieved data show reasonable estimation for snowfall rate compared with Cloudsat vertical image.

Key Words : Snowfall, CloudSat, Advanced Microwave Sounding Unit (AMSU), Microwave Humidity Sounder (MHS).

1. Introduction

Snowfall in the Korean region is a very important component in the climate system that plays a key role in the hydrological cycle. To monitor this snowfall, snowfall gauges and radar on the ground have been used, but these monitoring systems are difficult to implement and are sparsely distributed.

A satellite-based monitoring system is more effective for measuring snowfall over the Korean region. Passive microwave imaging radiometers operating at frequencies in which the atmosphere is relatively transparent have been available since 1978. Measurements onboard the EOS-Aqua satellite provide information about environmental parameters such as the areal extent of snow cover. Unfortunately,

Received May 26, 2011; Revised June 11, 2011, Revised June 23, 2011; Accepted June 24, 2011.
† Corresponding Author: Young-Seup Kim(kimys@pknu.ac.kr)

it is quite difficult for an AMSR-E sensor to measure the snowfall rates at a low frequency on the land area. In addition, there is little to be gained by incorporating passive visible or infrared measurements of Korean regions, since their effectiveness is limited to distinguishing clouds from bright surface ice during daytime viewing conditions. They would also introduce much ambiguity in many cases, such as when there are ice clouds over snow and sea ice, let alone in night time conditions. In recent years, researchers have shown an increased interest in developing an accurate snowfall rate from passive microwave measurements between 89-190 GHz from a NOAA AMSU-B sensor. The operational microwave radiometric sounders with "opaque" channels at frequencies in which the atmosphere absorbs radiation (such as the 183-GHz water vapor rotational absorption line) include the Microwave Humidity Sounder (MHS) and its predecessor, the Advanced Microwave Sounding Unit (AMSU-B), onboard the National Oceanic and Atmospheric Administration (NOAA) polar-orbiting platforms. The fact that the atmosphere obscures emissions from the underlying surface at these frequencies makes it plausible to try to use these channels to measure snow as it is falling in the atmosphere to use these channels to measure snow as it is falling in the atmosphere (Chen and Staeline, 2003; Jee and Lee, 2010; Kim *et al.*, 2008; Kim and Park, 2002; Kongili *et al.*, 2003; Liu, 2004; Noh *et al*, 2006; Shofronick-Jackson *et al.*, 2004).

The 94-GHz CloudSat Cloud profiling Radar (CPR) was launched in 2006 (Stephens *et al*, 2002). It can offer the first opportunity to date to provide systematic profiles of precipitation over Korean regions. The only polar-orbiting instrument that is directly sensitive to snowfall, the CPR has been collecting data over the Korean peninsula since June 2006. Its vertical profiles of radar reflectivity permit the systematic detection of any snowfall occurring within the instrument's field of view. Because the CPR has no scanning capability, it can only capture snow events that are directly beneath the track of CloudSat and this severely limits its sampling utility. This is why it is highly desirable to use direct CPR estimates to train the opaque-channel AMSU-B and MHS instruments in order to make estimates of snowfall within their wide 2300-km swaths. A priori, a passive radiometer alone is somewhat less than ideal for the estimation and monitoring of snowfall because its channels are only indirectly sensitive to the vertical distribution of any precipitation within its field of view. However, recent studies have confirmed that the measurements of these radiometers can indeed be used to detect such precipitation (Kongili *et al.*, 2003) and that their opaque and scattering channels are sensitive to falling snow (Bennartz and Bauer, 2003).

One can therefore expect that the best results would be obtained by selectively combining the measurements of all the passive channels, using the radar measurements to determine the most judicious combination, and to then estimate the column of condensed water, if not its detailed vertical profile, and to quantify the uncertainty of the estimates. The number and wide swath of the radiometers would then provide the sampling capability that CPR lacks. Our approach is to try to achieve this goal by correlating observed radiances with nearly-simultaneous radar profiles measured by the CloudSat radar.

2. Datasets and Procedures

The highest 3 channels of the AMSU-B sensor on board the NOAA satellite constitute the strongly water vapor absorption line. This is the operational humidity sounder on the NOAA-15, 16 and 17 spacecraft. Beginning with the launch of the NOAA-

18 spacecraft in 2005 and the ESA (European Space Agency) MetOp-A in 2006, AMSU-B was replaced with a similar Microwave Humidity Sounder (MHS). At each channel frequency, the antenna beamwidth is a constant 1.1 degrees (at the half-power point). Ninety contiguous scene-resolution cells are sampled in a continuous fashion, each scan covering each side of the subsatellite path. These scan patterns and the geometric resolution translate to a 16.3 km diameter cell at the nadir at a nominal altitude of 850 km. In order to establish a set of coincident CloudSat and AMSU-B/MHS measurements viewed under similar surface types, we used the AMSR-E instrument onboard the Aqua satellite. Since CloudSat observes in the a-train afternoon orbit and lags behind the Aqua satellite by approximately 90 seconds, these two satellites collect data almost simultaneously.

Cloud Profiling Radar (CPR) is a 94-GHz nadir-looking radar that measures the power backscattered by clouds as a function of the distance from the radar. CPR was developed jointly by NASA/JPL and the Canadian Space Agency (CSA). The overall design of the CPR is simple, well understood, and is strongly derived from many forms of cloud radar that are already in operation in ground-based and airborne applications.

The design of the CPR is driven by its scientific objectives. The original requirements of CPR were: sensitivity defined by a minimum detectable reflectivity factor of -30 dBZ, along-track sampling of 2 km, a dynamic range of 70 dB, 500 m vertical resolution, and a calibration accuracy of 1.5 dB. The minimum detectable reflectivity factor requirement was reduced to -26 dBZ when the mission was changed in order to put CloudSat into a higher orbit for formation flying. Fig. 1 shows the study area and a heavy snow image from Jan 2010 from the MODIS imager.

We used 2B-GEOPROF products. Cases of non-precipitation were discarded; the criterion for such a case was that the 2B-GEOPROF cloud mask flag never exceeded a value of 20. Finally, in order to

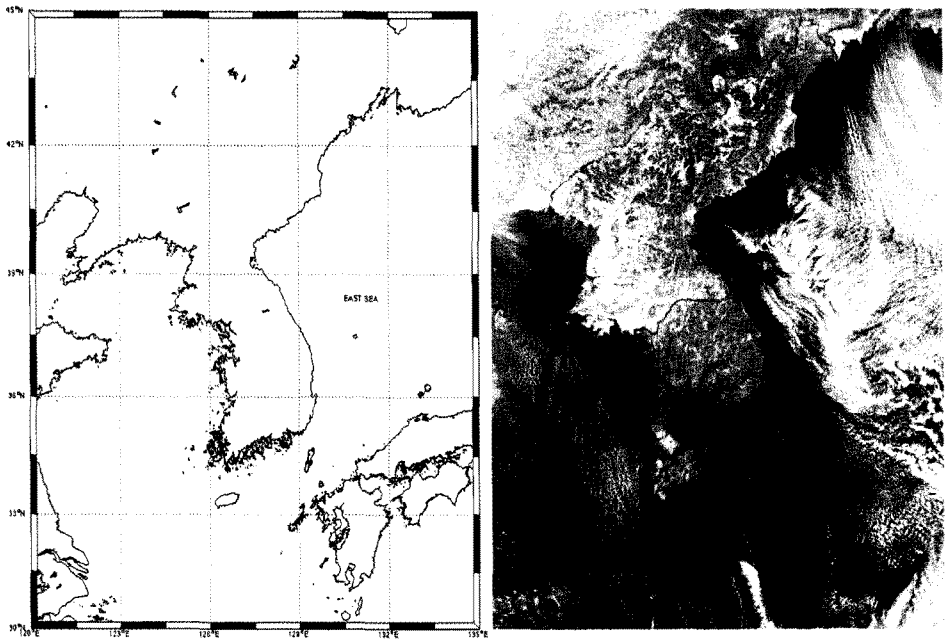

Fig. 1. Study area (left) and case image of heavy snow image in Jan 3. 2010 from MODIS rapid response system (right).

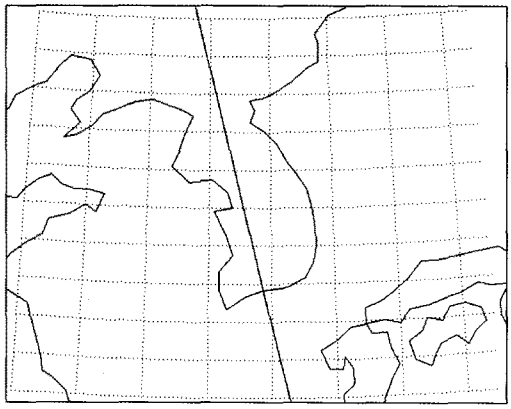

Orbit of CloudSat

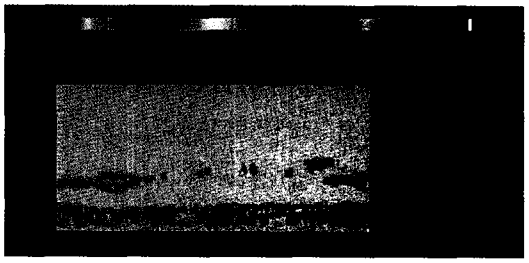

Cloud mask

Reflectivity

Fig. 2. Sample image for heavy snowfall by CloudSat in the Korean peninsula at 03:53 UTC Jan 20. 2010.

filter melting snow events, precipitation cases in which the vertical temperature profile exceeded -2° C (at any level in the profile) were discarded. Fig. 2 shows the vertical structure of a snowstorm in the Korean peninsula that was observed in Jan 2010.

We considered a CloudSat radar profile and a spatially co-located radiometer observation to be "simultaneous" if the difference between the times at which the two sets of data were acquired did not exceed 5 minutes. For each month beginning with Dec 2007 and ending Feb 2008, we compiled a database of co-located simultaneous CloudSat and AMSU-B measurements. To reduce the discrepancy between the radar resolution (about 1.4-km across-track, 1.7 km along-track) and the vastly coarser radiometer resolution, we averaged together the results of 15 consecutive CloudSat radar beams, the sequence being centered on the beam that fell closest to the coordinates of the center of the radiometer field of view. Each sample in the resulting database thus consists of a vector of 5 brightness temperatures and 40 radar reflectivity factors. The next section describes the method we used to relate the brightness temperatures to a snowfall proxy derived from the vertical radar profiles.

Lacking any substantial collection of ground-truth validation data from the Korea land region, we evaluate our approach by applying the relations derived from the databases built from data collected during one month of 2006 with the measurements in the same month of 2007 and 2008, along with the obvious permutations.

Our approach required that we tabulate the most nearly coincident measurements of CPR, on one hand, and of AMSU-B or MHS, on the other, into a database that would be representative of the range of values of the brightness temperatures in the radiometer channels that could correspond to a given radar measurement profile Z. While this approach is straightforward, it presents four issues that must be addressed.

Z is actually a vector that has as many entries as there are 500m vertical resolution bins in the precipitation column, though they are highly correlated and therefore cannot be considered to represent independent variables. How many independent variables would be required to represent this vector? Principal component analysis of the Tropical Rainfall Measurement Mission (TRMM) Precipitation radar data of all precipitation over the mid-latitude regions

sampled by TRMM indicates that the first principal component (essentially the average water content) accounts for over 80% of the variability, while the second accounts for another 10% or so (Coppens *et al*, 2000). Since it is highly unlikely that the variability of the vertical distribution of precipitation would be greater in Korean regions than over mid-latitude areas, we set ourselves the goal of estimating the first principal component of Z, while accepting the inevitable uncertainty that would remain because we ignored the higher principal components.

In order to collect a sufficient number of co-located radar and radiometer data, one will inevitably need to match observations of the same location that are made several minutes apart from one another. The effect of this delay will be built into the database. However, because some events will intensify in the interval and others will subside, the empirical relations derived from the database should eliminate the biases that this time discrepancy would cause.

In a relatively dry atmosphere, one would expect that all our high-frequency channels, including the opaque ones, would be affected by the variable surface emissivity. It is therefore important for our approach to include a mechanism that separates the variations that are due to the radiometric signatures of the condensation from those of the surface.

There is no single relation between the 94-GHz radar reflectivity Z and the underlying snow water content that holds for all snowfall, regardless of hydrometer type and size distribution. For this reason, we decided in this initial attempt to correlate the microwave sounder radiances with the reflectivity rather than with any dubious snow-rate retrieval.

The multi-parameter relations between radar reflectivity and the underlying snowfall rates can thus be studied independently, and the resulting retrieval can be appended as a final step to our passive-microwave retrieval of the radar principal component.

To minimize the effect of the variable surface emissivity on the measured radiances, our approach first analyzes the co-located radar and radiometer measurements in non-precipitation cases (as determined by the radar). We then use a principal component analysis to quantify the variability of the radiometer measurements over a given time interval and for each of surface conditions. We decided to first transform the five simultaneous radiometer radiances into five radiance-principal-components; these were indexed so that the first captures the bulk of the variability of the surface emissivity in a given class and during a given period. Our approach is to then discard this principal component, and use only the remaining combinations to match radiometer data with radar measurements when the latter indicates likely snowfall.

3. Retrieval Algorithm and Case Studies

For each of the surface-states discussed above, a Principal Component Analysis (PCA) was performed on the 5 frequency radiometer samples from the cloud-free profiles only (as determined by the simultaneous CloudSat profile).

$$\vec{T} \begin{pmatrix} T_1 \\ T_2 \\ T_3 \\ T_4 \\ T_5 \end{pmatrix} \xrightarrow{\text{PCA}} \vec{T'} \begin{pmatrix} T'_1 \\ T'_2 \\ T'_3 \\ T'_4 \\ T'_5 \end{pmatrix} W\vec{T} \qquad (1)$$

The PCA finds the orthogonal matrix that transforms $\vec{T}$ into a new set of five variables $\vec{T'}(W\vec{T'})$ whose components are uncorrelated and have been ranked according to the magnitude of their variance, whiche is in turn related to their contribution to the total variability of $\vec{T}$. Table 1 illustrates the results with the example of data collected. for each month beginning with Dec 2007 and ending Feb 2008 by the MHS radiometer on NOAA-18 from the Korean

Table 1. Mode values of clear sky for AMSU-B channels

	T_1	T_2	T_3	T_4	T_5
mode2	-0.408	0.412	0.203	0.352	0.703
mode3	0.289	-0.491	0.632	0.523	0.118
mode4	0.213	-0.490	-0.652	0.198	-0.499
mode5	-0.108	0.253	-0.364	0.749	-0.479

peninsula, and classified as cloud-free by the CloudSat radar data. The table shows the coefficients of the first cloud free principal component $\overrightarrow{T}$ for each month, Dec 2007, Jan 2008, and Feb 2008.

Since $\overrightarrow{T}$ capture most of the variability of the measured brightness temperature in cloud-free

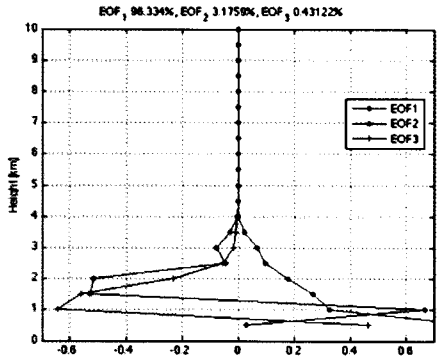

Land area in Jan 2008

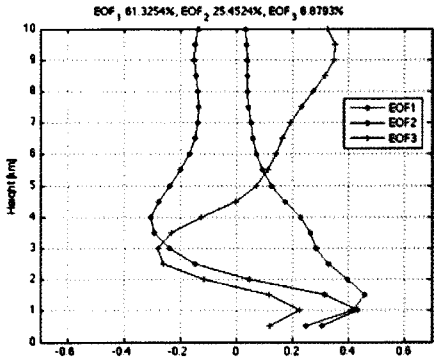

Land area in Feb 2008

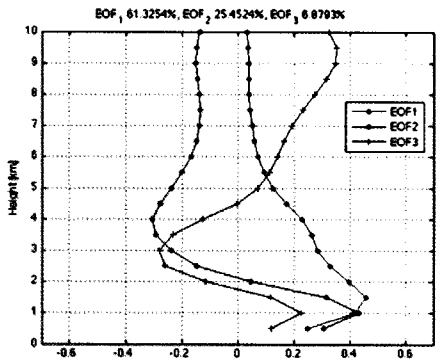

Ocean area in Jan 2008

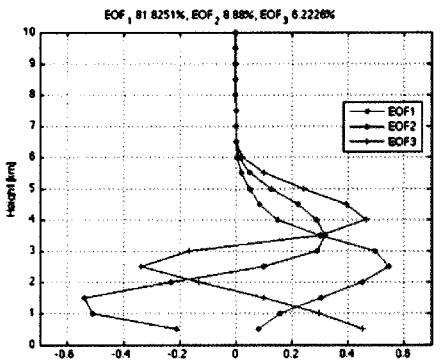

Ocean area in Feb 2008

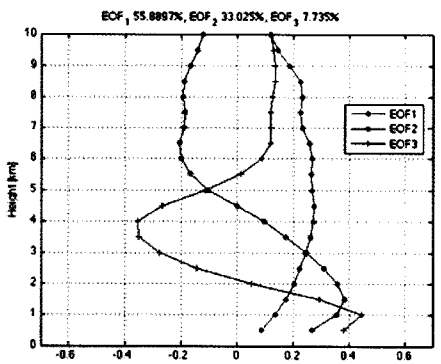

Study area in Jan 2008

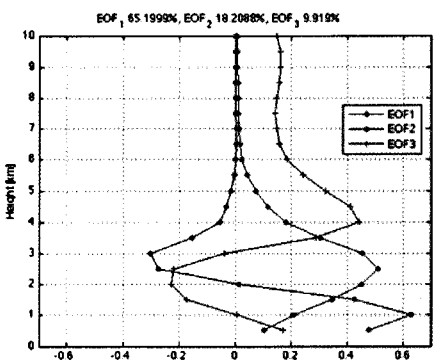

Study area in Feb 2008

Fig. 3. Coefficients of the first three vertical principal components of vertical radar reflectivity profiles.

conditions, the remaining four variables $\vec{T'}_2$, $\vec{T'}_3$, $\vec{T'}_4$, and $\vec{T'}_5$ must remain nearly constant in clear-sky cases. It is therefore reasonable to attribute their variability in precipitation to the signature of the precipitation, and hence to look for a relation between ($\vec{T'}_2$, $\vec{T'}_3$, $\vec{T'}_4$, $\vec{T'}_5$) and the vertical profiles of radar reflectivity measured by the CloudSat radar. Each CloudSat profile is a vector $\vec{Z}$ with 20 components, which represent the 94-GHz radar reflectivity factors measured in each of twenty consecutive 500-m vertical bins, starting at the surface. Fig. 3 illustrates the variability of these vertical distributions: the four panels show the first three principal components of $\vec{Z}$. In each case, the first component Z'_1 consists essentially of the average of the measured reflectivities below about 3km, plus a weighted average of the reflectivities above 3km with weights decreasing nearly linearly to 0 at the top of the column. This variable captures roughly 75% of the vertical variability, and the problem is to then quantify the extent to which it is correlated with($\vec{T'}_2$, $\vec{T'}_3$, $\vec{T'}_4$, $\vec{T'}_5$) and the extent to which any correlation can be used to estimate from ($\vec{T'}_2$, $\vec{T'}_3$, $\vec{T'}_4$, $\vec{T'}_5$) . There is no reason that the snowfall proxy Z'_1 should be linearly related to the radiometer principal components ($\vec{T'}_2$, $\vec{T'}_3$, $\vec{T'}_4$, $\vec{T'}_5$). For this reason, we first segmented the data within each class into five disjoint subclasses, which correspond to five contiguous intervals for Z'_1 that are defined using its mean μ_z and standard deviation σ_z as

C_1 : all samples with $Z'_1 < \mu_z$

C_2: all samples with $\mu_z < Z'_1 < \mu_z + 0.5\,\sigma_z$

C_3: all samples with $\mu_z + 0.5\,\sigma_z < Z'_1 < \mu_z + \sigma_z$

C_4: all samples with $\mu_z + \sigma_z < Z'_1 < \mu_z + 1.5\,\sigma_z$

C_5: all samples with $\mu_z + 1.5\,\sigma_z < Z'_1$

Within each subclass C_i, we looked for the four coefficients a_i, b_i, c_i, d_i and e_i that minimize the difference between the RMS of the left-hand-side and right-hand-side of

$$a_i + \alpha_1^{(i)} b_i T'_2 + \alpha_2^{(i)} c_i T'_3 + \alpha_3^{(i)} d_i T'_4 + \alpha_4^{(i)} e_i T'_5 = Z'_1 \quad (2)$$

Since each T' is a linear combination of the original brightness temperatures, we thus obtain coefficients $\alpha_1^{(i)}, \cdots\cdots \alpha_4^{(i)}, a_i$ which give the best piecewise-linear first for each segment C_i

Table 2. Coefficients $\alpha_1^{(i)}$, $\alpha_2^{(i)}$, $\alpha_3^{(i)}$, $\alpha_4^{(i)}$, a_i of the relations derived from February data.

	$\alpha_1^{(i)}$	$\alpha_2^{(i)}$	$\alpha_3^{(i)}$	$\alpha_4^{(i)}$	a_i
Jan 2008	0.04	-0.216	-0.16	-0.17	42.94
Feb 2008	-2.42	-0.767	-4.68	-0.78	750.80

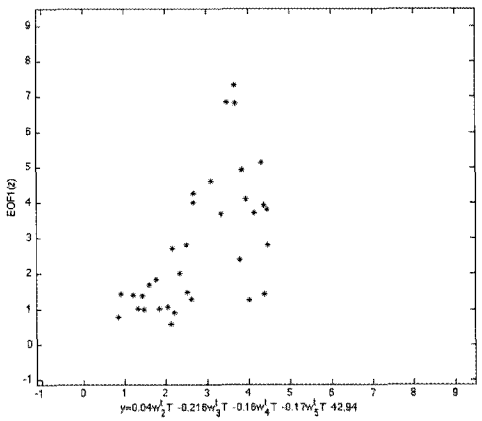

(a) Jan 2008

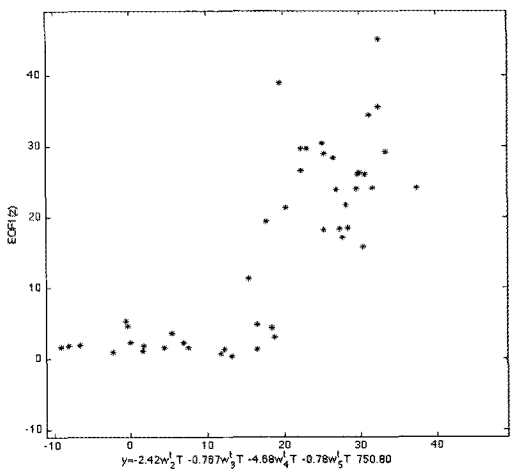

(b) Feb 2008

Fig. 4. Snowfall proxy (vertical axis) vs. regression-derived combination of brightness temperature over ocean in the Korean peninsula (a) Jan and (b) Feb 2008.

Table 2 illustrates the results from our running example of data from the Korea peninsula in the case class whose results were among the most consistent.

Fig. 4 plots our snowfall proxy Z'_1 from the measurements in the case in each year against the regressions derived from (a) Jan 2008 and (b) Feb 2008 over ocean of Korea. The plots shown for subclassC_1 - C_5 highlight that our samples of nearly simultaneous co-located measurements by CloudSat and NOAA-18 in each month in the presence of precipitation with an average reflectivity exceeding about 4.4 dBZ are scant for all data The fact that the

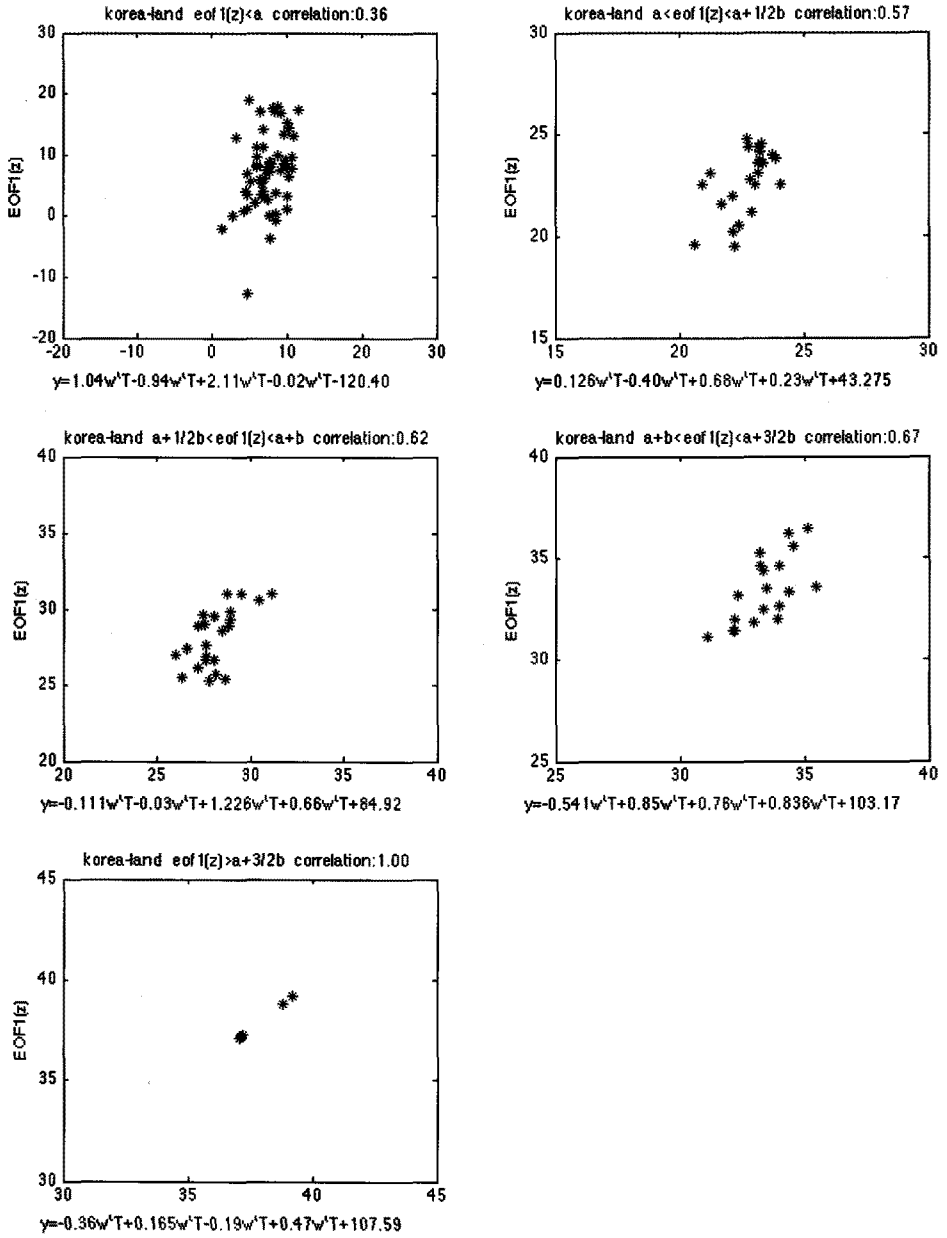

Fig. 5. Snowfall proxy (vertical axis) vs. regression-derived combination of brightness temperature for land of Korea.

weights of the given measurements are not identical in the four relations is not consistent with the fact that much of the vertical variability of the radar measurement is captured by Z'_1. Each of the four radiance principal components is correlated with the snowfall proxy, and there is no reason to expect a unique relation that would consistently perform better than all other possible linear combinations. In fact, a principal component analysis of the reflectivity profiles indicates that 3 variables are sufficient to capture over 90% of the variability of the snowfall, so one would expect some redundancy in the 4 radiance principal components.

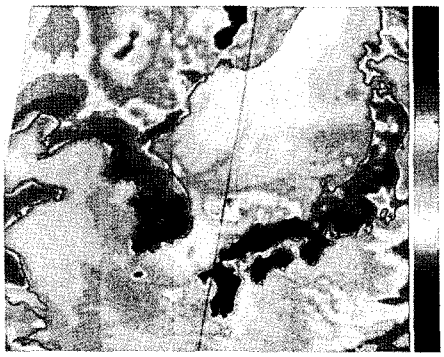

(a) 89.0 GHz

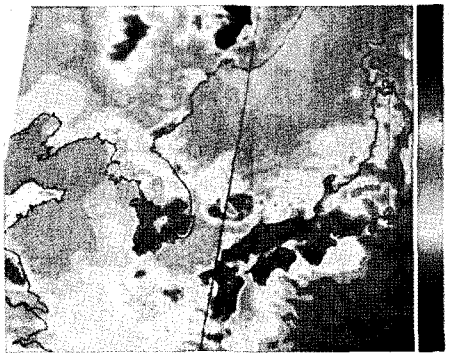

(b) 157.0 GHz

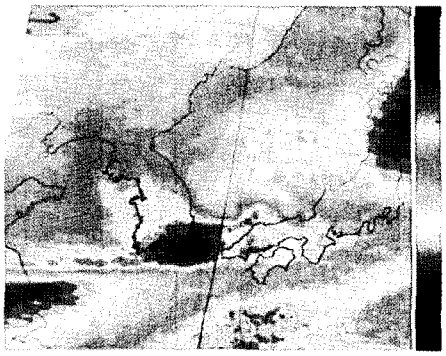

(c) 183±1 GHz

(d) 183±3 GHz

(e) 190 GHz

Fig. 6. Snow event from co-located measurements by CloudSat and NOAA-18 on Feb. 3, 2008.

Similarly, Fig. 5 plots our snowfall proxy Z'_1 against the regression derived for the radiometer measurements in each class, this time from 3 months of measurements over the land of Korea. The horizontal axis is the best combination for the subclasses C_1 (all samples with $Z'_1 < \mu_z$) in the left panel of first row, C_2 (all samples with $\mu_z < Z'_1 < \mu_z + 0.5\,\sigma_z$) in the right panel of the first row, C_3 (all samples with $\mu_z + 0.5\,\sigma_z < Z'_1 < \mu_z + \sigma_z$) in the right panel of the second row, C_4 (all samples with $\mu_z + \sigma_z < Z'_1 < \mu_z + 1.5\,\sigma_z$) in the right panel of the second row, and C_5 (all samples with $\mu_z + 1.5\,\sigma_z < Z'_1$) in the bottom panel. There is no useful correlation in the low-Z'_1 class. The middle panel suggests the beginning of a distinct relation, and a clear correlation is apparent in the high-Z'_1 subclass.

The development of falling snow is applied to the heavier snowfall case around the East Sea in the Korean peninsula. Fig. 6 shows the brightness temperature from five AMSU-B channels from $89,157,183 \pm 1,183 \pm 3$ and 190GHz with the vertical profile of the observed CloudSat 94GHz reflectivity (2B-GEOPROF) associated with the overpass tracks within 5 minutes. In particular, a heavy snowfall band is located near the city of Pohang, as has occurred during heavy rainfall for several years.

Fig. 7. Case study of and instantaneous retrieval of snowfall proxy during one orbit of NOAA-18 on 15:50 UTC Feb. 3, 2008.

Finally, the snowfall retrieval algorithm is applied to the NOAA satellite. The snowfall case which is studied is located over the East Sea and takes place in Feb 3 2008, as shown by Cloudsat measurement of heavy snowfall. Fig. 7 shows the case of an instantaneous retrieval of the snowfall proxy during one orbit of NOAA-18 in 15:50 UTC Feb 2008. The retrieval algorithm clearly shows that the snow band coincided with the Cloudsat vertical reflectivities.

4. Conclusions

We have developed snowfall retrieval algorithm and illustrated the synergistic use of high frequency satellite data in conjunction with Cloudsat radar overpasses to provide wintertime snowfall estimateions.

The results showed that the high-frequency microwave passive measurements from operational sounders such as the AMSU-B and MHS can reproduce the precipitation sensitive radar reflectivities measured by the CloudSat radar over Korean regions. The results could be more optimized if the surface were classified based on the variability of its clear-sky emissivity, and the surface effect were minimized by identifying and eliminating the main principal component of the clear sky radiances. The method and results presented above illustrate the extent to which high-frequency microwave passive measurements from operational sounders such as the AMSU-B and MHS can reproduce the precipitation-sensitive radar reflectivities measured by the CloudSat radar over Korean regions, once the surface has been at least coarsely classified according to the variability of its clear-sky emissivity, and once the effect of the latter has been minimized by identifying

and eliminating the main principal component of the clear-sky radiances. We performed the principal component analyses on the snowfall and the brightness temperatures from high frequency sensors implying that Gaussian statistics govern the joint behavior of these variables. This approach should improve the performance of the retrieval algorithm.

Our approach treats the CloudSat radar vertical profiles of snowfall as the reference against which the passive measurements are trained. In particular, this approach allows us to separate the problem of relating the passive radiances to the radar measurements from the problem of retrieving snowfall rate profiles from 94-GHz radar reflectivity profiles.

We concluded that our retrieval algorithm can retrieve the detailed information reasonably about vertical distribution of snowfall from the observations of a multi-frequency active and passive microwave sensors such as Cloudsat and AMSU-B satellite. Snowfall retrieval algorithm applied to brightness temperature of AMSU-B to estimate snowfall rate for snowstorm over East Sea during Feb 2008. In general, our retrieval algorithm reproduces very similar snowfall patterns with Cloudsat vertical image. We are plan to apply our algorithm to the heavy snowfall cases over land with the ESA and NASA cloud radar mission such as Earth Care and ACE(Aerosol-Cloud-Ecosystem).

Acknowledgements

This work was supported by a National Research Foundation of Korea (NRF) grant funded by the Korean government (MEST) (No.2010-0016871).

References

Bennartz, R. and P. Bauer, 2003. Sensitivity of microwave radiances at 85-183 GHz to precipitation ice particles. *Radio Sci.* 38(8075), doi:10.1029/2002RS002626.

Chen, F. W. and D. H. Staeline, 2003. AIRS/AMSU/HSP precipitation estimates, *IEEE Trans. Geosci. Remote Sens.*, 41: 410-417, doi:10.1109/TGRS.2002.808322.

Coppens, D., Z. S. Haddad, and E. Im, 2000. Estimating the uncertainty in passive microwave rain retrievals. J. Atmos. *Ocean. Tech.*, 17: 1618-1629.

Stephens, G. L., D. G. Vane, R. J. Boain, G. G. Mace, K. Sassen, Z. Wang, A. J. Illingworth, E. J. O'connor, W. B. Rossow, S. L. Deruden, S. D. Miller, R. T. Austin, A. Benedetti, C. Mitrescu, and the Cloudsat Science Team, 2002. The CloudSat mission and the A-Train. *Bull. Amer. Meteor. Soc.*, 83: 1771-1790.

Jee, J. B. and K. T. Lee, 2010. Estimation of rainfall intensity for MTSAT-1R data using microwave rainfall. *Korean Journal of Remote Sensing*, 26(5): 511-525.

Kim, M.-J., J. A. Weinman, W. S. Olson, D.-E. Chang, G. Skofronick-Jackson, and J. R. Wang, 2008. A physical model to estimate snowfall over land using AMSU-B observations, *J. Geophys. Res.*, 113: D09201, doi:10.1029/2007JD008589.

Kim, Y. S. and K. W. Park, 2002. Rainfall estimation using TRMM-PR/VIRS and GMS data, *Korean Journal of Remote Sensing*, 18(6): 319-326.

Kongili, C., P. Pellegrino, R. R. Ferraro, N. C. Grody, and H. Meng, 2003. A new snowfall detection algorithm over land using measurements from the Advanced Microwave Sounding Unit (AMSU), *Geophys. Res. Lett.*, 30(14): 1756,

doi:10.1029/2003GL017177.

Liu, G., 2004. Approximation of single scattering properties of ice and snow particles for high microwave frequencies, *J. Atmos. Sci.*, 61: 2441-2456, doi:10.1175/1520-0469(2004) 061<2441:AOSSPO>2.0.CO;2.

Noh, Y.-J., G. Liu, E.-K. Seo, J.R. Wang, and K. Aonashi, 2006. Development of a snowfall retrieval algorithm at high microwave frequencies, *J. Geophy. Res.*, 111: D22216, doi: 10.1029/2005JD006826.

Skofronick-Jackson, G., M.J. Kim, J. Weinman, and D. Chang, 2004. A physical model to determine snowfall over land by microwave radiometry, *IEEE Trans. Geoscience Rem. Sens.*, 42(5): 1047-1058.